Effects of Coastal Upwelling and Downwelling on Hydrographic Variability and Dissolved Oxygen in Mobile Bay

Jeffrey Coogan[1], Brian Dzwonkowski[1], and John Lehrter[1]

Jeffrey Coogan, Jcoogan@disl.org

[1]Department of Marine Sciences,

University of South Alabama, Dauphin

Island Sea Lab, Dauphin Island, Alabama,

USA.

This article has been accepted for publication and undergone full peer review but has not been through the copyediting, typesetting, pagination and proofreading process, which may lead to differences between this version and the Version of Record. Please cite this article as doi: 10.1029/2018JC014592

Abstract. Upwellling and downwelling events are important coastal processes that strongly influence shelf ecosystem dynamics. Though changes on the shelf have been well studied, the impact of these events on estuarine systems has received less focus. In summer 2016 a downwelling and upwelling event were observed near the mouth of Mobile Bay. The impact of these events were examined throughout the bay with high spatial resolution observations. Five boat surveys were conducted to capture the spatial response of offshore forcing and its changes in the estuary. In addition to the surveys, 16 CTDs were deployed and measured temporal changes. A 7°C temperature change was observed in the channel as a result of the offshore changes. In the shipping channel and offshore, advection was a major source of changes in heat content and often exceeded the surface heat flux. Advection of low dissolved oxygen water into the estuary was also observed in the shipping channel and at the Dauphin Island station nearest to the estuary mouth. The extent of these changes highlights the importance of estuary-shelf connectivity in river-dominated systems where offshore forcing can drive large changes in estuaries during low flow summer conditions.

Keypoints:

- Heat Flux observations highlight large differences in heat content associated with advection from offshore upwelling and downwelling events.
- Small thermal eddy diffusivity values are associated with stratification in the estuary.

- Advection of low dissolved oxygen water from the shelf into the estuary

was observed in the shipping channel and near the estuary mouth.

1. Introduction

Hydrodynamic variability in many estuarine systems is dominated and controlled by changes in river forcing and the estuarine circulation driven by changes in density gradients. These upstream sources dictate the level of freshwater input that forces circulation dynamics, as well as the variability of salinity, temperature, nutrients, sediment, and pollutants in these semi-enclosed systems. On the offshore end of estuaries, the coastal variability is often thought of as a secondary driver of changes in these systems. This is especially true in river dominated systems where high discharge rates can drive low residence times and dominate estuary dynamics. The offshore influence can become more important though as offshore variables such as temperature change with respect to the estuary. These changes in the nearshore region have been observed to drive low frequency variability in estuaries around the world [*Barton et al.*, 2015; *Hickey*, 2002; *Schroeder and Wiseman*, 1986]. The offshore change can impact both the barotropic and baroclinic components of estuary forcing and may need to be considered when examining river dominated estuaries.

The mechanisms driving offshore hydrographic variability at the coastal boundary are often associated with upwelling and downwelling events. *Barton et al.* [2015] observed these changes in a semi-enclosed bay, Ria de Vigo, Spain, where persistent upwelling and downwelling resulted in waters from the continental shelf driving changes in temperature 10 km up estuary. *Monteiro and Largier* [1999] also found that the offshore variability from upwelling events drove temperature changes in the estuary, and that these changes led to increased baroclinic pressure gradients between the coastal region and bay in South

Africa. The changes resulted in density driven exchange that was three times faster than tidal exchange alone. In addition to the offshore changes, periods of low discharge were found to be an important component in assessing the estuary response to offshore forcing. *Hickey* [2002] observed in Willapa Bay, Washington that variability in the estuary was a result of changes offshore during periods of low discharge. These previous studies have highlighted the importance of connectivity, changes in forcing conditions, and mechanisms of offshore variability driving changes in estuarine systems.

The importance of this offshore forcing can be magnified during low flow when longer residence times occur in estuaries. This offshore change can also impact biogeochemical pathways in estuaries. Advection of low dissolved oxygen water from offshore was observed by *Fujiwara* [2002] and *Brown and Nelson* [2015] and is a central component of determining the oxygen budget in estuaries. Material transfer from offshore is another important aspect of this variability, where large concentrations in chlorophyll can be advected into estuaries as a result of upwelling [*Roegner and Shanks*, 2001]. Other environmentally important material transport from offshore includes pollutants and oil.

Previous observations of offshore forcing's impact on estuaries have primarily focused on the barotropic component through remote wind forcing [*Wong and Moses-Hall*, 1998; *Gong et al.*, 2009; *Feng and Li*, 2010]. In Mobile Bay *Schroeder and Wiseman* [1986] observed this same forcing occurring in the estuary on the order of a few days as a result of Ekman convergence and divergence on the coast. The work also highlighted the importance of the shipping channel as a conduit to estuarine-shelf exchange. In October 2015, *Cambazoglu et al.* [2017] observed a large influx of high salinity shelf water into Mobile Bay and Mississippi Sound also due to Ekman transport continuously flowing and trapping

water inside the bay. These previous observations have focused on water level changes driving the variability and barotropic flow. During the summer low discharge periods occur in Mobile Bay while offshore enhanced Ekman transport associated with strong stratification occurs on the Alabama shelf at the mouth of Mobile Bay [*Dzwonkowski et al.*, 2011a]. This combination of long residence times, strong baroclinic circulation, and offshore variability suggest additional changes associated with the baroclinic flow are likely to occur in Mobile Bay.

This study aims to highlight the importance of offshore variability and the connectivity between the near shore region and estuary based on observations from Mobile Bay where data were collected during one downwelling and two upwelling events. Previous research has focused on direct forcing through changes in water level and the barotropic component of offshore forcing. This study focuses on changes in the baroclinic component, and regions of the bay impacted. The offshore variability has important implications for heat flux, baroclinic forcing, and bottom water dissolved oxygen concentrations. Observations from summer 2016 highlight how offshore changes impact shallow estuaries and the extent, and pathways of intrusion in these systems.

2. Data and Methods

2.1. Study Site

Mobile Bay is a shallow microtidal estuary of the northern Gulf of Mexico. The tidal system is diurnal and averages 0.4 m. The relatively shallow uniform bathymetry averages 3 m and can be observed in Figure 1, where the 5 m contour shows very little change throughout the bay. The exception to this is the 12 m deep, 120 m wide shipping channel that runs the length of Mobile Bay. The bay is relatively large extending 48 km long

and ranging from 14-34 km wide. Exchange with the gulf is constricted to two relatively narrow passes: Main Pass controlling an estimated 64% of the exchange [*Kim and Park*, 2012] and Pass Aux Herons connecting to Mississippi Sound.

Mobile Bay has the fourth largest river discharge in the continental US [*Kammerer*, 1990] with an average discharge of 1,516 m^3s^{-1} from 2000-2016. During summer and early fall the average river discharge falls to less than 500 m^3s^{-1}, and the length of the estuary (measured by the 6 PSU contour) can extend beyond the city of Mobile at the northern end of the bay [*Coogan and Dzwonkowski*, 2018]. During this low discharge period the bay can have residence times of up to 30 days, compared with 4 days during peak discharge events [*Du et al.*, 2018].

Offshore of Mobile Bay is the Mississippi-Alabama shelf, a highly stratified system. In summer, the average vertical temperature and salinity differences are $\sim$4°C and a 5 PSU [*Dzwonkowski et al.*, 2011b]. Instantaneous values can be much larger, and unpublished measurements from summer 2018 observed a salinity difference of 10-12 PSU. This wide shallow shelf system is generally forced by wind driven currents [*Dzwonkowski and Park*, 2012]. At synoptic time scales, the current structure has characteristic wind-driven Ekman response and the effectiveness of this across-shelf transport can be enhanced by stratification on the shelf [*Dzwonkowski et al.*, 2011a, 2014].

2.2. Data Sources

Several data sets were compiled to provide observations of how offshore variability impacted Mobile Bay during 1 downwelling and 2 upwelling events that occurred in the summer of 2016. Figure 1 highlights these compiled data sources: offshore mooring (ma-

roon dot), estuary water quality stations (red dots), hydrographic survey transects (dash lines), and additional offshore hydrographic survey sites (yellow dot).

The offshore mooring is comprised of a thermistor chain, near surface CTD, and upward looking ADCP. The site is located approximately 25 km west southwest of the Mobile Bay main pass (site CP in Figure 1). The mooring is maintained by the Dauphin Island Sea Lab and has been collecting data since 2004. The thermistor chain is made up of 5 Seabird SBE 56 temperature loggers collecting data at 1 min intervals and positioned at 6, 9, 11, 14, and 16 m from the surface. A Seabird MicroCAT measured salinity and temperature at 4.7 m from the surface every 20 mins. Temperatures near the surface (> 4.7 m) and near the bottom (< 18.5 m) were assumed constant in calculating the depth averaged temperatures at Station CP. An RDI 600 kHz ADCP collected current data over 5 min burst every 20 mins at 0.5 bins between 2 and 18 m from the surface. The ADCP also collected temperature data 0.5 m above the sea floor. A low pass 48-hour Lanczos filter was used to isolate the subtidal changes that occurred offshore during the upwelling and downwelling conditions. To calculate the offshore flow structure the across-shelf transport (North/South) was calculated following *Dever* [1997] by removing the depth averaged across-shelf velocity and integrating from the surface to the first zero crossing of the low-pass filtered current profile:

$$T_s(t) = \int_0^{\zeta} (v(z,t) - V(t))dz \tag{1}$$

where T_s is the across-shelf surface transport, z is the depth, ζ is the depth of the first zero crossing, v is the subtidal across-shelf velocity component, and V is the depth-averaged across-shelf velocity. Velocities near the surface (< 2 m) and below the last bin (> 18 m) were assumed constant in calculating the across-shelf transport. The across-

shelf transport was set as positive onshore (northward) and negative offshore (southward) with no coordinate transformation and was in agreement with previous work in the area [*Dzwonkowski et al.*, 2011a].

Sixteen water quality stations collected salinity, temperature, dissolved oxygen, and pressure data throughout the bay. Data was collected using YSI 6600s and the water quality stations included long-term monitoring sites maintained by the Dauphin Island Sea Lab, and Alabama Marine Resources Division, and short-term deployments that collected data from July 12, 2016 to August 2, 2016. Long-term data from station DI was also analyzed from July 2006 to September 2017. Fifteen of the stations were fixed near bottom sites 0.25-0.5 m above the sea floor. The only non fixed station was MB (in the center of the bay Figure 1) that collected vertical profile data at 0.5 m intervals throughout the water column. Data was collected at 60, 30, and 10 min frequencies based on the site and were subsequently averaged to hourly data for processing.

Five hydrographic boat surveys were conducted to examine the spatial and temporal variability of salinity, temperature, and dissolved oxygen in the bay. The five surveys were conducted during the month of July on the 14th, 19th, 21st, 28th, and 30th. Each survey involved measuring vertical profiles with a Seabird SBE 25 in the channel and on the shoals of 5 transects, shown in Figure 1 as dashed lines and labeled A to E. Due to weather and time limitations not all 5 transects could be completed during each survey. Surveys of all 5 lines took between 6-8 hours to complete (1/3-1/4 of the tidal cycle). A total of 266 vertical profiles were collected to provide excellent spatial observations throughout the bay. In addition to the five bay wide boat surveys, opportunistic data from three Dauphin Island Sea Lab student cruises (7/11, 7/14, and 7/19) was included

to expand the data set. The CTD profiles that overlapped with the study site transects were used when available, and an additional offshore site (DO) was added to examine offshore dissolved oxygen changes. The CTD profiles measured salinity, temperature, and dissolved oxygen with a Seabird SBE 25.

Meteorological data were collected offshore at NOAA station 42012, and inshore data was collected at station MB in the center of the Bay. Offshore wind speed and direction were collected 4 m above sea level and corrected to 10 m. The offshore wind data was then low passed filtered with a 48-hour Lanczos filter and used to asses upwelling and downwelling conditions offshore. Solar radiation, air temperature, humidity, barometric pressure, and wind speed were measured at the MB station and used to calculate surface heat flux. Wind speed and direction was collected 14.2 m above sea level and corrected to 10 m. Meteorological data were collected every minute and averaged to hourly data for processing.

2.3. Heat Budget

To examine the changes in temperature that occurred in the estuary two heat budget equations were used: a 1-D heat budget and a diffusion heat budget. The 1-D heat budget compared the observed changes in heat content measured in the bay (left hand side of Eq 2) with those estimated from a 1-D solution (right hand side of Eq 2), where surface flux is the only source term, and advection of heat in the along- or cross-shore direction is neglected. Following *Fewings and Lentz* [2011] the change in depth-average water temperature $\langle T \rangle$ is a result of changes in the surface heat flux Q_{surf}:

$$\langle T(t_2) \rangle - \langle T(t_1) \rangle = \frac{1}{\rho_0 c_p h} \int_{t_1}^{t_2} Q_{surf}(t) dt \tag{2}$$

where ρ_0 is the depth-average density, t is time, h is water depth, and c_p is the specific heat capacity of seawater and equal to $4,010\text{Jkg}^{-1}\text{C}^{-1}$. The observed changes in heat content ($\langle T(t_2)\rangle - \langle T(t_1)\rangle$) were calculated from the timeseries profiles at the offshore site, CP, and from the timeseries profiles from the center of Mobile Bay at site MB. In addition to the timeseries data, changes in heat content were also measured between hydrographic boat surveys using CTD temperature profiles to quantify spatial changes in the heat flux, where t_1 and t_2 are hydrographic survey dates and their subsequent heat content from the temperature profiles. The profiles change in heat content were solved for at each survey station and also grouped by area (channel, east bay, west bay, and bay wide) shown in Figure 3.

Observations of temperature changes in the bay were compared with the 1-D heat flux solved using:

$$Q_{surf} = Q_E + Q_H + Q_S + Q_L \tag{3}$$

where Q_E is latent heat flux, Q_H is sensible heat flux, Q_S is shortwave heat flux, and Q_L is longwave heat flux. Latent, sensible, and shortwave heat fluxes were solved using meteorological observations at station MB, and longwave heat flux was estimated using the North American Regional Reanalysis (NARR) model developed by NOAA. The bulk flux for sensible and latent heat flux was calculated using the MATLAB$^{\text{TM}}$ toolbox developed by *Pawlowicz et al.* [2001]. Shortwave heat flux was measured directly at station MB with a solar radiation sensor and 10% of the incoming radiation was assumed to be reflected by the bays albedo based on average NARR model outputs for this region. The NARR model outputs also provided daily longwave heat flux estimates that were interpolated and used to calculate hourly heat flux observation estimates.

The second heat budget equation used to quantify the changes observed in the estuary was a diffusion heat budget and calculated the rate of heating for a volume of water below the pycnocline. Two timeseries stations (MB-SD, MB-CW, CW-NT, and CW-BB) were used to mark the peak of the cold-water intrusion event. It was assumed that these peaks were measuring the same water mass as it was advected through Mobile Bay. From a Lagrangian observation, this near bottom cold water mass below the pycnocline will be heated by diffusion. This heating was solved by Fickian diffusion,

$$\frac{\partial \overline{T}}{\partial t} = -K_z \frac{\partial^2 \overline{T}}{\partial z^2} \tag{4}$$

and used to solve a discrete equation that calculated an estimated eddy diffusivity (K_z), where the changes in temperature between two stations ($\partial \overline{T}/\partial t$) was equal to the time and temperature change between peaks in cold water for the two stations, and the temperature gradient $\partial^2 \overline{T}/\partial z^2$ was solved using surface data from the MB station and near bottom temperature data from the second station. This technique provided first order estimates of diffusion, and a method for analyzing potential pathways of intrusion in this shallow estuary. Assumptions in this method do not account for horizontal dispersion that are likely an additional source of heating and result in smaller diffusivities than those observed with this method. The limits of this assumption are expanded on in further detail in the discussion.

3. Results

3.1. Offshore Changes

During the summer 2016 observation period, offshore data at station CP captured one downwelling (7/25) and two upwelling (7/6 & 8/10) events (Figure 3). The start and

end of events were defined by the along estuary winds. The first upwelling event started at the beginning of July and persisted through the 11th. During this upwelling period the along-shore winds were moderate, averaging 1.7 ms^{-1} and peaked at 5.1 ms^{-1}. This wind forcing drove an offshore surface transport of -0.12 m^2s^{-1} and peaked at -0.60 m^2s^{-1}. Temperatures associated with this upwelling period averaged 24.1°C and dropped as low as 22.4 °C. The second upwelling event was similar in length beginning in early August and lasting till the 13th. The average along-shore wind velocity was comparable at 1.4 ms^{-1}, but had a higher max wind velocity of 7.2 ms^{-1}. The average surface transport was also greater, -0.19 m^2s^{-1}, but had a lower peak of -0.48 m^2s^{-1}. Temperature changes were smaller with a warmer lowest observed temperature of 23.6 °C and average of 25.9 °C.

The downwelling event was shorter in time than both upwelling events and occurred from July 24th to the 26th. Along-shore wind velocities were higher than those associated with the upwelling events and averaged 3.0 ms^{-1} with a max velocity 9.1 ms^{-1}. These higher winds forced a surface transport that peaked at 1.01 m^2s^{-1} and averaged 0.43 m^2s^{-1}. Temperatures associated with this downwelling event averaged 28.4°C with a lowest observed temperature of 24.0°C.

3.2. Bay Wide Observations

During the same period of offshore observations, timeseries data and hydrographic surveys were examined to capture the impact and variability that offshore changes had on the estuary (Figure 4 and 5). CTD casts from the channel (Figure 4) shows the changes in temperature and salinity that occurred between 7/11 and 7/30. The cast colors are also shown in Figure 3a as vertical lines, where five of the cast occurred after the 1st

upwelling event and two occurred after the downwelling event. The coldest water can be seen entering the bay on July 11th at transects E, D and C (note transect A was not surveyed on 7/11 and 7/14, and Transect B was not surveyed on 7/11), where the colder water was at transect E and D nearest to the mouth of Mobile Bay. In addition to the cold water, the salinity profiles showed that higher salinities near the bottom of the channel were also present. Three days later (7/14) the coldest temperatures were observed at transect D, C, and B, with Transect E beginning to warm and salinity drop. This warming and salinity drop was likely a result of the subtidal circulation driving the cold high salinity water further up estuary as the channel water near the mouth was replaced by warming lower salinity water from offshore. Figure 5a also captured this trend where both the depth average offshore temperature ($CP_{DepthAvg}$ maroon line) began warming on 7/11 and also the temperature change in the channel began warming (blue and red dots). Ten days after the offshore upwelling event (7/21), traces of cold water and higher salinities could still be observed in the channel at transects A and B (Figure 4, 28 km into the estuary. Around this same time the northern timeseries stations (BB, NT, and SD) showed their drop-in temperature (Figure 5). Following the downwelling period more uniform temperatures and less salinity variability were observed throughout the channel with some of the warmest temperatures occurring in the bottom of the channel on 7/28 at transects C, B, and A.

With the observed changes in temperature and salinity, along-estuary density gradients were also changing in response to the offshore variability. Table 1 shows the density gradients solved for the eastern and western sides of the bay, and along the channel based on the hydrographic survey CTD profile data (note that the surveys took 6-8 hours to

complete and gradients may reflect some tidal variability in this diurnal system). Focusing on the channel data, a large gradient occurred on 7/11 at the peak of the upwelling event. Three days later (7/14), a negative gradient occurred as the cold saltwater intrusion moves up-estuary (north) in the channel. Low gradients continued on the 19th and 21st in the channel as the dense cold saltwater was replaced with warmer lower salinity water near the mouth of the channel. The larger density gradients then return on the 28th and 30th. Low and negative density gradients were also observed bay wide on the eastern and western sides of the estuary following the cold-water intrusion event but showed higher values on the 19th and 21st. Timeseries data were also used to calculate the changes in density gradients from the most northern (MP) and southern (DI) water quality stations. Table 1 shows very little change in the density gradient between these sites during the six survey dates when compared to the CTD profile based gradients.

Timeseries data from all the water quality stations throughout the bay also highlighted these temperature changes, though not as strongly as the observations from the channel (dots show channel data in Figure 5a). Figure 5a shows moderate changes leading up to and following the first upwelling event (7/6), where the largest changes occurred at CW and MB stations nearest the channel. This warming continued up to the first downwelling event, where all the timeseries stations in the bay had comparable temperatures after 7/25. The varied response of the bay to upwelling events was observed during the second upwelling event on 8/14, where Figure 5a shows a drop in temperature at all the stations (with the exception of SD). This change in response was associated with higher wind velocities and changes in surface heat flux (Figure 5c) that occurred during the second

upwelling event and resulted in two unique bay wide responses in the timeseries data to upwelling events.

3.3. Heat Flux

Temperature change in the bay was examined with a heat flux equation to quantify the differences between observations and a 1-D heat budget solution (Eq 2). Deviations from the 1-D heat budget indicated the relative importance of advection in the heat budget for different areas of the bay. No deviation indicated surface heating was the only source driving the net temperature signal. Figure 5b shows the timeseries of heat content observations for a central site in the bay (MB), and the offshore mooring location, CP (it should be noted MB in Figure 5a was near bottom temperature and MB in Figure 5b was solved over the entire water column).

Station MB was in 4m of water and tracked closely with the 1-D heat budget solution. The largest observed deviations occurred around August 10, the second downwelling event. In comparison with station MB, CP exhibited more variability and deviations from the 1-D heat budget where upwelling and downwelling drive large swings in the heat content for this nearshore region. Following the 7/6 upwelling event, Figure 5b shows large changes offshore at site CP as the upwelling relaxes, transitions to downwelling (7/25) and then back to upwelling. The largest change in heat flux could be seen on 7/26, just after the downwelling event. The mean difference between the 1-D heat budget solution and station MB was -33.5 Wm^{-2} with a standard deviation of 88.3Wm^{-2}. By comparison the offshore site had a lower mean difference, -13.5 Wm^{-2}, and higher standard deviation, 296.3Wm^{-2}.

The heat content changes throughout the estuary between hydrographic surveys were also compared and shown in Table 2, and plotted in Figure 6. Table 2, similar to Figure 5b, shows that the largest variability in heat flux occurred offshore and in the shipping channel. In the channel, the heat flux exceeded the surface flux on the surveys following the upwelling event, as warm water from the shelf was advected into the bay replacing the cold upwelled water. Bay wide changes showed similar trends with the surface flux but were on average 40 wm^{-2} less than the surface flux values. The data shows the advective heat flux offshore (20m depth) and in the shipping channel (12-15m depth) was at times the dominate component driving change, but bay wide (3m average depth) had less of an impact on temperature when compared to the surface heat flux.

The importance of advection in the shipping channel could also be observed in Figure 6, where the change in heat content for individual CTD profiles are shown. Profiles from the channel are identified as open circles, and all other profiles outside the shipping channel are solid dots. As previously mentioned, the bay wide changes showed a similar trend to the surface flux but were on average 40 wm^{-2} less than the surface flux values. This offset could be seen in Figure 6 as the difference between the dashed line (1-D heat budget solution) and the solid dots (change in heat content observations outside the shipping channel). Values from the channel showed greater variability when compared to the 1-D solution as a result of the shelf-estuary advection associated with changes offshore driving variability in the heat content.

3.4. Intrusion Timescales and Diffusivity

With the large swings in temperature the cold-water mass could be used as a tracer to estimate the time and diffusion rates for Mobile Bay. Three timeseries stations near the

channel were examined to estimate the cold-water peak: MB, CW, and SD. Station MB reached its lowest temperature (26.0° C) at 5:40 on July 13th followed by CW (27.7° C) at 22:40 on the 13th, and lastly SD (27.9 ° C) at 11:00 on July 15th. With the event peaking offshore on July 10th it took approximately 5 days for the cold-water mass to travel the 48 km estuary length. Using these time lags, estimated subtidal velocities range from 6.3 to 15 cms^{-1}. The time lag velocities were comparable to those estimated by *Hansen and Rattray Jr* [1966] analytical solution for subtidal exchange, where an eddy viscosity of $0.001 m^2 s^{-1}$ and the density gradients from Table 1 (MP to DI) predict near bottom subtidal velocities that range from 8.7 to 10.5 cms^{-1}.

The observations in this study highlight the channel's importance as a pathway for the cold-water intrusion observed deep in the shipping channel. Cold water observations in the shallow regions of the bay (Figure 7) prompted further questions of the dominate pathway for this water mass (spilling out of the channel laterally or along estuary exchange within the shallow region of the estuary) and the importance of stratification reducing thermal eddy diffusivity.

To determine the likely pathway Eq 4 was calculated to solve for the thermal diffusion based on the time lag between two points. The two points were selected based on a path of either along-estuary transport (offshore station as S1 and a shallow region station as S2) and lateral transport from the channel (station near the channel as S1 and the shallow region station as S2). These two pathways could then be compared to determine the more likely intrusion pathway based on how plausible the calculated diffusivities were. Table 3 shows the estimated diffusion for each pathway examined. The two pathways had comparable values and provided little insight on the likely dominate pathway of intrusion

(neither values were outside of the expected range of thermal eddy diffusivity values). The small thermal eddy diffusivity values highlighted the importance of stratification in Mobile Bay where the depth average salinity gradient at station NT was 3.2 PSUm^{-1} and as high as 10.6 PSUm^{-1} at the pycnocline . This strong stratification was associated with the low thermal eddy diffusivities of 6.31×10^{-5} and 1.09×10^{-4} m^{2}s^{-1} in the northeast region of the bay.

3.5. Dissolved Oxygen

In addition to temperature being advected from offshore, observations in the shipping channel captured changes in dissolved oxygen associated with the changing offshore conditions. Figure 8 shows three offshore profiles taken from hydrographic surveys 17 km east of station CP (Station DO in Figure 1, the larger dot highlights the area over which these measurements were made). The three profiles were measured during the end of the upwelling event (7/11), just after (7/14), and several days after (7/19). During the event the near bottom dissolved oxygen reached a minimum of 1.5 mgL^{-1} and was hypoxic in the bottom 2.4 m of the water column. Three days later there was a large change in dissolved oxygen and little change in the salinity and temperature profile. The max vertical density gradient decreased from 13.4 to 4.3 kgm^{-4}, and indicated changes in dissolved oxygen may be responding faster to ambient conditions post upwelling than temperature and salinity. This may also have been reflecting changes in the response to relaxation of the isopycnals post upwelling, where the upward tilted isopycnals associated with upwelling relaxed and adjust to changes in the wind. It should be noted that the profile on 7/11 was measured at 09:04 and on 7/14 at 13:40 where light and local biological oxygen sources and sinks may impact the observed values. Eight days after the event the profile on 7/19 measured little

change in oxygen concentration with depth as the offshore conditions began transition to the downwelling event and lower stratification occurred offshore.

Measurements from the channel during this same time period (Figure 9) showed large changes in dissolved oxygen occurred between 7/11 (the end of the upwelling event) and 7/19 (the start of the downwelling event). The starting concentration of the dissolved oxygen near the mouth of the bay resulted in lower initial concentrations as the water moves up-estuary through the channel. Using a Lagrangian approach this change in oxygen was calculated based on the initial concentration at the mouth of the estuary and compared with the nearest station at the next survey date in time using a subtidal velocity of 6.3 cms^{-1} calculated in section 3.4. The depth-integrated dissolved oxygen flux was then calculated to be -1.67 (7/11-7/14), -1.16 (7/14-7/19), -1.98 (7/19-7/21), and 0.124 $gO_2m^{-2}d^{-1}$ (7/28-7/30) . No dissolved oxygen rate was able to be calculated between 7/21 and 7/28. The three dissolved oxygen rates calculated before 7/21 show a loss in the shipping channel and after 7/28 a small gain. On July 26 there was a strong wind event that decreased stratification in the bay (Figure 4 7/21-7/28) and this decrease in stratification was likely enough to increase vertical mixing of dissolved oxygen producing a positive oxygen flux on 7/28-7/30.

Observations outside the shipping channel at the timeseries stations in Mobile Bay showed a range of dissolved oxygen trends associated with the upwelling and downwelling periods as a result of a number of potentially important physical, chemical, and biological changes that occurred throughout the bay. The results of the clearest trend were at the DI station and are focused on to understand the potential impacts of offshore changes on dissolved oxygen in the estuary. Figure 10b shows the relationship between temperature

and dissolved oxygen measured at station DI near the mouth of the bay during July 2016. The observed trend between dissolved oxygen and temperature highlights that the low temperature water associated with the upwelling was advecting with it low dissolved oxygen from offshore into this region of the bay. This cold water at station DI was also associated with saltier water from the upwelling event (Figure 10a).

To further highlight the importance of this trend, 11 years of temperature and dissolved oxygen measurements from the month of July were plotted in Figure 10c. The correlation for all of July 2006-2017 (blue dots) was 0.14 ($P< 0.001$). Red dots in the same figure show only periods associated with strong upwelling events, where the correlation increased to 0.52 ($P< 0.001$). The strong upwelling periods were selected based on a threshold condition of 4 day periods with an average offshore surface transport greater than 0.005 m^2s^{-1}. Additionally, an 11 hour time lag was added for the dates selected as strong upwelling periods, based on sensitivity analysis.

4. Discussion and Conclusions

4.1. Coastal Variability

Observations from summer 2016 captured the offshore changes that can occur on the Alabama-Mississippi shelf as a result of both upwelling and downwelling events. These offshore events drove a depth averaged temperature change of 4.3°C at site CP. The changes in temperature and salinity reflect previous work by *Dzwonkowski et al.* [2011b, a] who observed upwelling and downwelling conditions can be common on this wide shallow shelf as a result of high stratification in the summer and calmer wind conditions that reduce mixing.

The summer stratification is an important component in enhancing across-shelf wind driven Ekman transport [*Lentz*, 2001; *Dzwonkowski et al.*, 2011a]. The strong vertical salinity and temperature gradients offshore at CP were also observed by *Dzwonkowski et al.* [2011b] to continue through the nearshore region and into the estuary. This strong stratification between the estuary and shelf is likely enhancing the connectivity of the two regions through tilting of isopycnals near the mouth of Mobile Bay and the associated across-shelf wind driven Ekman transport.

The Alabama-Mississippi shelf has limited research highlighting the spatial extent of these offshore changes. *Dzwonkowski and Park* [2012] observed along-shelf currents were highly coherent with wind, but across-shelf velocity is generally not as a result of the estuary driving changes in coastal currents. Other work by *Dzwonkowski et al.* [2015] found that Mobile Bay can have a large impact on the shelf. This estuary shelf forcing is often associated with high discharge periods, as discharge decreases in the bay the roles switch and offshore changes begin to play a larger role in impacting the estuary. This estuary-shelf connection is often dominated by one side but may also lead to feedbacks as these two end members drive changes that impact each other.

A growing body of work on dissolved oxygen changes in the northeast region of the Gulf of Mexico has shown the region east of the Mississippi River Delta is susceptible to hypoxia development in the summer months [*Brunner*, 2006; *Milroy*, 2016; *Dzwonkowski et al.*, 2018]. A large focus of previous work has been on stratification and river nutrients driving low dissolved oxygen. In 1998, a hydrographic survey of the northeastern Gulf of Mexico by *Nowlin et al.* [2000] observed patterns of onshore movement of nutrient-rich bottom waters and associated low dissolved oxygen. The dissolved oxygen bottom

concentrations were spatially variable though across the shelf from the 1,000m contour to shore. Work by *Feng et al.* [2014] showed wind can enhance the evolution of summer hypoxia on the Louisiana-Texas shelf in the northern Gulf of Mexico, and may provide another mechanism for low dissolved oxygen associated upwelling observed in this study. In strong upwelling regions like California and Oregon, researchers have observed event scale changes in dissolved oxygen associated with upwelling events [*Frieder et al.*, 2012; *Grantham et al.*, 2004; *Connolly et al.*, 2010]. The trends and limited observations near Mobile Bay make discerning the upwelling of low dissolved oxygen observations in this region important for establishing the occurrence of these changes, though long-term likelihood of these events is difficult to discern. Previous studies have noted that physical factors can enhance (wind, stratification, strength of upwelling), and reduce (advection, mixing) the dissolved oxygen trend [*Adams et al.*, 2013] , and are likely important on the Alabama-Mississippi shelf as well. This work highlights the system connectivity between what is happening on the shelf and surrounding estuaries.

4.2. Estuary Variability

During the 2.5 weeks of hydrographic surveys a 7°C temperature swing was observed in this shallow estuary with the warmest temperatures at one point occurring at the bottom of the 12 m deep shipping channel after a downwelling event. The implications of this connection between offshore variability and the impact on the estuary are clearly seen in the channel, and additional temperature changes in some regions of the bay may be more impacted than others. By using the large temperature swing as a tracer, the time lag between stations could be used to estimate subtidal velocities and thermal eddy diffusivity rates.

The time lag derived subtidal velocities in the channel were comparable to simple analytical theory. *Du et al.* [2018] found near bottom subtidal velocities in the channel of Mobile Bay that were 10cms^{-1} with numerical modeling and are also comparable to those found in this study. Modeling results by *Du et al.* [2018] also found that subtidal near bottom velocities and ocean flux continue to increase with discharges up 2,000m^{3}s^{-1}. This increase in velocity and large ocean flux indicates the offshore changes may continue to strongly impact the bay beyond low discharge changes and should be examined in future work.

Changes in density (Table 1) indicate that the bay wide density gradient (station MP to DI) changed little during the 2.5 weeks of observations. Shorter spatial scales indicate notable variability did occur in the strength and direction of the bays density gradients. In the channel, density gradients dropped to zero, and were negative as the slug of dense upwelled water made its way through the estuary. No current measurements were made in the channel, but the data suggest subtidal current velocities in the shipping channel may have been highly variable over this 2.5-week period. The barotropic component of the momentum balance has been observed as an important term in offshore forcing on estuaries [*Schroeder and Wiseman*, 1986; *Garvine*, 1985; *Wong and Garvine*, 1984], and this work highlights how the baroclinic term is also being impacted. The role of baroclinic vs barotropic importance from offshore forcing is less clear in the data. Since the barotropic component is easier to observe, a large focus of previous work has examined it. The opportunistic observations made in this study show the baroclinic component is driving changes in the system and the relative importance of these forcing components due to offshore changes should be investigated in future work. Evidence of enhanced baro-

clinic forcing have been previously observed by *Monteiro and Largier* [1999] and *Hickey* [2002]. The reduction in density gradients following the upwelling event has received less attention, and additional changes may be impacting the estuary with respect to any material (plankton, nutrients, pollutants) advected into the estuary after an upwelling event that may not circulate as quickly due to the drop-in the density gradient observed in this study.

With good agreement between the time lag of temperature changes and subtidal velocity estimates, temperature changes were also used to calculate the thermal eddy diffusivity in Mobile Bay. Similar methods of thermal diffusivity calculations have been used in lakes where no horizontal or vertical advection is assumed [*Jassby and Powell*, 1975]. This study assumed the peak in cold water at two stations showed the same water mass being advected through the bay, and was examined from a Lagrangian reference frame. Diffusivity estimates measured this way are comparable to the lower range of measurements made by *Peters and Bokhorst* [2001] that encompassed 5×10^{-2} to 5×10^{-5}m^{2}s^{-1}. The aim of this technique was to improve the understanding of pathways in the bay. Since both pathways had similar diffusivities little insight on the dominate pathway was gained. The results highlight the importance of stratification in this shallow bay and provide a mechanism for the cold water observed in Figure 7 to be present at the height of summer in this subtropical estuary.

The diffusivity method used did not account for horizontal diffusion, which has been observed by *Monismith et al.* [2009] as a potentially large source of heat transfer in other systems. An estimate of this term is O(10^{-5}) based on observed horizontal temperature gradients and a horizontal diffusivity of 100 compared with O(10^{-5}) for the vertical diffu-

sivity. Though this source was assumed negligible, it would provide an additional source of heat transport, and the vertical diffusivity estimates in this study are likely smaller than those reported due to the horizontal diffusion. The temperature values measured in the shallow regions of the bay and timeseries data highlight the connection between offshore temperature changes and the shallow regions of the estuary, particularly the eastern side of the bay highlighted in Figure 7. The persistence of this colder water is thought to be largely due to stratification in the bay, as the water is slow to warm due to high stratification and low diffusivity. Transects that occurred early in the morning also highlight the magnitude of this response where temperature inversions develop overnight and can be seen in the profiles throughout the bay.

Measurements of the heat content showed that the heat budget in Mobile Bay was comparable to the 1-D estimates (Figure 5b and 6). Bay wide there are no large fluctuations when compared with the 1-d heat flux and observed changes (Table 2). These results do not indicate advection is not important in the bay, but rather any heat flux associated with subtidal exchange is balanced and has no net effect in the estuary. In the channel and offshore are where the large differences occur due to advection. Model results by *Du et al.* [2018] in Mobile Bay estimate with a river discharge of $426 m^3 s^{-1}$ (the average in this study was $306 m^3 s^{-1}$) the offshore influx into the system is $700 m^3 s^{-1}$. This level of transport and the average offshore upwelling temperature have an advective heat flux of $6.3 W m^-2$ for the entire bay. The results in Table 2 show considerably larger changes occur in the channel as a result of this offshore advection being concentrated within the smaller volume of the channel.

The MB timeseries observations in Figure 5b and bay wide in Table 2 have an approximate offset of $\sim 33 - 40 \mathrm{Wm}^{-2}$ between the observed heat content change and the surface heat flux. Since the offset occurs during both upwelling and downwelling it is likely that the difference is associated with an error in measuring heat flux at the surface or advection sources not accounted for from the river or ground water. If the source of error is associated with the surface heat flux calculation then the offshore site, CP, would also be impacted. The offshore average difference in Figure 5b was $13.5 \mathrm{Wm}^{-2}$ and indicates the potential error in measuring heat flux at the surface is likely $\sim 13.5 \mathrm{Wm}^{-2}$ and can be accounted for in the various terms in Eq 3. Ground water input in Mobile Bay has been estimated to be $15 \mathrm{m}^3\mathrm{s}^{-1}$ by *Montiel and Dimova* [2017], and would only contribute $0.22 \mathrm{Wm}^{-2}$ at 20°C. *Monismith et al.* [2009] observed a similar offset of around $100 \mathrm{Wm}^{-2}$, and concluded it was from advection associated with river discharge. No upstream temperature data were available for this study but temperatures at the northern most water quality station (SD) are on average warmer than the bay, and does not provide a source of cooling. Additional sources of error include the bulk estimates associated with the sensible and latent heat lux, albedo, and bottom heat loss. This relatively constant offset does show an important source of error in calculating heat fluxes in the bay and potentially similar estuary systems. The heat flux offset observed is likely a result of contributions from all the sources mentioned above.

Advection of low dissolved oxygen water into Mobile Bay has not been previously observed and is likely an important component of dissolved oxygen trends near the mouth of the estuary and in the shipping channel. Data outside the channel and away from the main pass showed less correlation with respect to the offshore changes as other terms in

the dissolved oxygen budget drive variability. Offshore profiles had low dissolved oxygen on July 11th and data highlights that this low dissolved oxygen was advected into the shipping channel driving the observed changes. The shipping channel has its lowest dissolved oxygen values during the upwelling event and hypoxic conditions occur farther up estuary as a result of local changes in the oxygen budget. The offshore variability being advected into the bay and local changes have comparable loss rates and this results in making bay wide trends difficult. The dissolved oxygen measured in the channel showed decreasing trends with distance from the mouth of the estuary (Figure 9). The average oxygen loss prior to 7/28, 1.60 $gO_2m^{-2}d^{-1}$, was comparable to previous observations made in the bay that ranged from 1.1-2.0 $gO_2m^{-2}d^{-1}$ [*Park et al.*, 2007], and sediment oxygen consumption rates of 0.1-1.25 $gO_2m^{-2}d^{-1}$ [*Cowan et al.*, 1996]. This importance of oxygen consumption vs advection highlights the complexity of the oxygen budget in estuaries. Observations at station DI indicate the upwelling events on the coast are often advecting low dissolved oxygen water into the estuary. The correlation observed is impacted by both physical factors influencing the upwelling strength and biogeochemical factors offshore influencing the dissolved oxygen concentration associated with upwelling.

4.3. Conclusion

Two major components, stratification and subtidal circulation, are identified as important elements in this study to predict the offshore influence on estuarine variability. The observations in this study captured the offshore changes in temperature, salinity, and dissolved oxygen that can occur and impact shallow stratified estuaries. The offshore events drove a 7°C temperature swing over a 17-day period in Mobile Bay. The largest changes were restricted to the channel and highlight the importance of the shipping channel in

facilitating this pathway. Shallow systems with deep shipping channels (e.g. Galveston Bay, Texas and Tampa Bay, Florida) are likely to have this same pathway connecting offshore variability and changes in the estuary.

The temperature and salinity changes drove variability in the baroclinic forcing at kilometer scales in the estuary that may result in changes in the subtidal circulation. This understudied reduction of baroclinic forcing may have important impacts on other biological and chemical changes advected into the bay from an upwelling event, where materials advected into the estuary may slow down with circulation after the event and lead to increased residence times for the upwelled material, including oil pollutants, low dissolved oxygen water, nutrients, and plankton blooms.

Each of the offshore events led to varying responses in the bay. The temperature changes after the first upwelling event were subtle and mainly restricted to the channel. The second upwelling event resulted in a large bay wide change in temperature that corresponded with the offshore change, a drop-in surface heat flux, and stronger wind mixing. The lack of measurements in the channel for the second upwelling event also made comparison observations less clear but data from the first event suggest the estuary-shelf connection is likely just as important during the second event.

Understanding coastal variability is important not just for the nearshore circulation but as seen in this study can result in large hydrographic changes in shallow systems beyond barotropic setup. The temperature and dissolved oxygen changes observed in Mobile Bay highlight this importance of estuary-shelf connectivity and future research should focus on improving our understanding of chemical and biological differences associated with the offshore water entering river dominated estuaries.

Acknowledgments. Data were collected by the Tech Support Group at the Dauphin Island Sea Lab, including Kyle Weis, Roxanne Robertson, Alan Gunter, Mike Dardeau, G. Lockridge, Hunter King, Y. Hintz and L. Linn and the Alabama Realtime Coastal Ocean Observing System program manager, R. Collini (Data available at `www.mymobile.com`). Dauphin Island Sea Lab student cruise were led by Dr. Jeff Krause, Dr. Behzad Mortazavi, Maddie Kennedy, and Liesl Cole. Additional data sources were also made available by the Alabama Department of Natural Resources−Marine Resource Division. This research was made possible in part by a grant from The Gulf of Mexico Research Initiative, and in part by NOAA Restore program(NA17NOS4510101), and Alabama Department of Conservation and Natural Resources - Marine Resources Division. Data are publicly available through the Gulf of Mexico Research Initiative Information & Data Cooperative (GRIIDC) at `https://data.gulfresearchinitiative.org` [doi:10.7266/n7-s40s-3785], the NOAA national centers for environmental information at `https://data.nodc.noaa.gov/cgi-bin/iso?id=gov.noaa.nodc:0176497`, and from other public sources at `http://www.ndbc.noaa.gov/` and `https://www.disl.org/research/data-management-center`.

References

Adams, K. A., J. A. Barth, and F. Chan (2013), Temporal variability of near-bottom dissolved oxygen during upwelling off central Oregon: summer DO variability on Oregon shelf, *Journal of Geophysical Research: Oceans*, *118*(10), 4839–4854, doi:10.1002/jgrc.20361.

Barton, E., J. Largier, R. Torres, M. Sheridan, A. Trasvia, A. Souza, Y. Pazos, and A. Valle-Levinson (2015), Coastal upwelling and downwelling forcing of circulation in a semi-enclosed bay: Ria de Vigo, *Progress in Oceanography*, *134*, 173–189, doi:10.1016/j.pocean.2015.01.014.

Brown, C. A., and W. G. Nelson (2015), A method to identify estuarine water quality exceedances associated with ocean conditions, *Environmental Monitoring and Assessment*, *187*(3), doi:10.1007/s10661-015-4347-3.

Brunner, C. A. (2006), Hypoxia Hotspots in the Mississippi Bight, *The Journal of Foraminiferal Research*, *36*(2), 95–107, doi:10.2113/36.2.95.

Cambazoglu, M. K., I. M. Soto, S. D. Howden, B. Dzwonkowski, P. J. Fitzpatrick, R. A. Arnone, G. A. Jacobs, and Y. H. Lau (2017), Inflow of shelf waters into the Mississippi Sound and Mobile Bay estuaries in October 2015, *Journal of Applied Remote Sensing*, *11*(3), 032,410, doi:10.1117/1.JRS.11.032410.

Connolly, T. P., B. M. Hickey, S. L. Geier, and W. P. Cochlan (2010), Processes influencing seasonal hypoxia in the northern California Current System, *Journal of Geophysical Research*, *115*(C3), doi:10.1029/2009JC005283.

Coogan, J., and B. Dzwonkowski (2018), Observations of Wind Forcing Effects on Estuary Length and Salinity Flux in a River-Dominated, Microtidal Estuary, Mobile Bay, Alabama, *Journal of Physical Oceanography*, *48*(8), 1787–1802, doi:10.1175/JPO-D-17-0249.1.

Cowan, J. L., J. R. Pennock, and W. R. Boynton (1996), Seasonal and interannual patterns of sedimentwater nutrient and oxygen fluxes in Mobile Bay, Alabama (USA): regulating factors and ecological significance, *Marine Ecology Progress Series*, pp. 229–245.

Dever, E. P. (1997), Wind-Forced Cross-Shelf Circulation on the Northern California Shelf*, *Journal of Physical Oceanography*, *27*(8), 1566–1580, doi:10.1175/1520-0485(1997)027⟨1566:WFCSCO⟩2.0.CO;2.

Du, J., K. Park, J. Shen, B. Dzwonkowski, X. Yu, and B. I. Yoon (2018), Role of Baroclinic Processes on Flushing Characteristics in a Highly Stratified Estuarine System, Mobile Bay, Alabama, *Journal of Geophysical Research: Oceans*, doi:10.1029/2018JC013855.

Dzwonkowski, B., and K. Park (2012), Subtidal circulation on the Alabama shelf during the Deepwater Horizon oil spill: subtidal circulation on Alabama shelf, *Journal of Geophysical Research: Oceans*, *117*(C3), n/a–n/a, doi:10.1029/2011JC007664.

Dzwonkowski, B., K. Park, and L. Jiang (2011a), Subtidal across-shelf velocity structure and surface transport effectiveness on the Alabama shelf of the northeastern Gulf of Mexico, *Journal of Geophysical Research*, *116*(C10), doi:10.1029/2011JC007188.

Dzwonkowski, B., K. Park, H. Kyung Ha, W. M. Graham, F. J. Hernandez, and S. P. Powers (2011b), Hydrographic variability on a coastal shelf directly influenced by estuarine outflow, *Continental Shelf Research*, *31*(9), 939–950, doi:10.1016/j.csr.2011.03.001.

Dzwonkowski, B., K. Park, J. Lee, B. M. Webb, and A. Valle-Levinson (2014), Spatial variability of flow over a river-influenced inner shelf in coastal Alabama during spring, *Continental Shelf Research*, *74*, 25–34.

Dzwonkowski, B., K. Park, and R. Collini (2015), The coupled estuarine-shelf response of a river-dominated system during the transition from low to high discharge: Estuarine-shelf rsponse to discharge, *Journal of Geophysical Research: Oceans*, *120*(9), 6145–6163, doi:10.1002/2015JC010714.

Dzwonkowski, B., S. Fournier, J. Reager, S. Milroy, K. Park, A. Shiller, A. Greer, I. Soto, S. Dykstra, and V. Sanial (2018), Tracking sea surface salinity and dissolved oxygen on a river-influenced, seasonally stratified shelf, Mississippi Bight, northern Gulf of Mexico, *Continental Shelf Research*, *169*, 25–33.

Feng, Y., K. Fennel, G. A. Jackson, S. F. DiMarco, and R. D. Hetland (2014), A model study of the response of hypoxia to upwelling-favorable wind on the northern Gulf of Mexico shelf, *Journal of Marine Systems*, *131*, 63–73, doi:10.1016/j.jmarsys.2013.11.009.

Feng, Z., and C. Li (2010), Cold-front-induced flushing of the Louisiana Bays, *Journal of Marine Systems*, *82*(4), 252–264, doi:10.1016/j.jmarsys.2010.05.015.

Fewings, M. R., and S. J. Lentz (2011), Summertime cooling of the shallow continental shelf, *Journal of Geophysical Research*, *116*(C7), doi:10.1029/2010JC006744.

Frieder, C. A., S. H. Nam, T. R. Martz, and L. A. Levin (2012), High temporal and spatial variability of dissolved oxygen and pH in a nearshore California kelp forest, *Biogeosciences*, *9*(10), 3917–3930, doi:10.5194/bg-9-3917-2012.

Fujiwara, T. (2002), Inflow of oceanic water into Tokyo Bay and generation of a subsurface hypoxic water mass, *Journal of Geophysical Research*, *107*(C5), doi:10.1029/2000JC000749.

Garvine, R. W. (1985), A simple model of estuarine subtidal fluctuations forced by local and remote wind stress, *Journal of Geophysical Research: Oceans*, *90*(C6), 11,945–11,948.

Gong, W., J. Shen, K.-H. Cho, and H. V. Wang (2009), A numerical model study of barotropic subtidal water exchange between estuary and subestuaries (tributaries) in

the Chesapeake Bay during northeaster events, *Ocean Modelling*, *26*(3-4), 170–189, doi:10.1016/j.ocemod.2008.09.005.

Grantham, B. A., F. Chan, K. J. Nielsen, D. S. Fox, J. A. Barth, A. Huyer, J. Lubchenco, and B. A. Menge (2004), Upwelling-driven nearshore hypoxia signals ecosystem and oceanographic changes in the northeast Pacific, *Nature*, *429*(6993), 749–754, doi:10.1038/nature02605.

Hansen, D. V., and M. Rattray Jr (1966), Gravitational circulation in straits and estuaries.

Hickey, B. M. (2002), Coupling between the California Current System and a coastal plain estuary in low riverflow conditions, *Journal of Geophysical Research*, *107*(C10), doi:10.1029/1999JC000160.

Jassby, A., and T. Powell (1975), Vertical patterns of eddy diffusion during stratification in Castle Lake, California1: Vertical eddy diffusion, *Limnology and Oceanography*, *20*(4), 530–543, doi:10.4319/lo.1975.20.4.0530.

Kammerer, J. (1990), Largest Rivers in the United States, *U.S. Geological Interview, Department of the Interior: Washington, DC*, *Open-File Report 87-242*.

Kim, C.-K., and K. Park (2012), A modeling study of water and salt exchange for a micro-tidal, stratified northern Gulf of Mexico estuary, *Journal of Marine Systems*, *96-97*, 103–115, doi:10.1016/j.jmarsys.2012.02.008.

Lentz, S. J. (2001), The Inuence of Stratication on the Wind-Driven Cross-Shelf Circulation over the North Carolina Shelf, *Journal of Physical Oceanography*, *31*, 12.

Milroy, S. (2016), Frequency of hypoxia at artificial reefs within the Mississippi Sound and Bight, 585 Jun-Oct 2016., Biloxi, MS.

Monismith, S. G., J. L. Hench, D. A. Fong, N. J. Nidzieko, W. E. Fleenor, L. P. Doyle, and S. G. Schladow (2009), Thermal Variability in a Tidal River, *Estuaries and Coasts*, *32*(1), 100–110, doi:10.1007/s12237-008-9109-9.

Monteiro, P., and J. Largier (1999), Thermal Stratification in Saldanha Bay (South Africa) and Subtidal, Density-driven Exchange with the Coastal Waters of the Benguela Upwelling System, *Estuarine, Coastal and Shelf Science*, *49*(6), 877–890.

Montiel, D., and N. Dimova (2017), Effects of small-scale hydrogeologic heterogeneity on submarine groundwater discharge (SGD) dynamics in river dominated estuaries: example of Mobile Bay, Alabama.

Nowlin, W., A. Jochens, M. Howard, S. DiMarco, and W. Schroeder (2000), Hydrographic properties and inferred circulation over the northeastern shelves of the Gulf of Mexico during spring to midsummer of 1998, *Gulf of Mexico Science*, *18*(1), 40–45.

Park, K., C.-K. Kim, and W. W. Schroeder (2007), Temporal variability in summertime bottom hypoxia in shallow areas of Mobile Bay, Alabama, *Estuaries and Coasts*, *30*(1), 54–65.

Pawlowicz, R., B. Beardsley, S. Lentz, E. Dever, and A. Anis (2001), Software simplifies air-sea data estimates, *Eos, Transactions American Geophysical Union*, *82*(1), 2–2, doi:10.1029/01EO00004.

Peters, H., and R. Bokhorst (2001), Microstructure Observations of Turbulent Mixing in a Partially Mixed Estuary. Part II: Salt Flux and Stress, *Journal of Physical Oceanography*, *31*, 15.

Roegner, G. C., and A. L. Shanks (2001), Import of Coastally-Derived Chlorophyll a to South Slough, Oregon, *Estuaries*, *24*(2), 244, doi:10.2307/1352948.

Schroeder, W. W., and W. J. Wiseman (1986), Low-frequency shelf-estuarine exchange processes in Mobile Bay and other estuarine systems on the northern Gulf of Mexico, in *Estuarine Variability*, pp. 355–367, Academic Press, Inc., New York.

Wong, K.-C., and R. W. Garvine (1984), Observations of wind-induced, subtidal variability in the Delaware estuary, *Journal of Geophysical Research: Oceans*, *89*(C6), 10,589–10,597.

Wong, K.-C., and J. E. Moses-Hall (1998), On the relative importance of the remote and local wind effects to the subtidal variability in a coastal plain estuary, *Journal of Geophysical Research: Oceans*, *103*(C9), 18,393–18,404, doi:10.1029/98JC01476.

Table 1. Average density gradients $kgm^{-3}km^{-1}$ based on hydrographic survey data in the channel, the western and eastern side of the bay, and timeseries data at the northern and southern most timeseries stations.

	7/11/2016	7/14/2016	7/19/2016	7/21/2016	7/28/2016	7/30/2016
Channel	0.156	-0.0153	0.050	0.077	0.148	0.114
East Bay	N/A	0.008	0.168	0.198	0.262	0.215
West Bay	N/A	-0.019	0.450	0.338	0.227	0.366
DI to MP	0.3202	0.314	0.290	0.269	0.351	0.319

Table 2. Average heat content change between survey dates, where the largest changes are in the channel and bay wide changes are relatively consistent and on average 40Wm^{-2} less than the surface flux.

	7/14-7/19	7/19-7/21	7/21-7/28	7/28-7/30
Surface Flux	57.1	77.5	13.5	78.8
Bay Wide	5.2	36.7	-15.3	36.4
Channel	330.5	246.5	-6.1	90.2
East	3.4	36.0	-21.6	26.2
West	1.7	34.1	-11.5	42.2
Offshore (CP)	198.5	178.8	208.4	-54.5

Table 3. Estimated eddy diffusivity values in Mobile Bay calculated using Eq 4 between two timeseries stations (S1 & S2) and from offshore to S2, using the peak cold-water event as a tracer to calculate the warming below the pycnocline from diffusivity.

S1	S2	S1 to S2 time lag (days)	Offshore to S2 time lag (days)	S1 to S2 lateral diffusion (m^2s^{-1})	Offshore to S2 along-estuary diffusion (m^2s^{-1})
MB	SD	2.22	4.46	2.62×10^{-5}	2.76×10^{-5}
MB	CW	0.71	2.94	6.47×10^{-5}	3.49×10^{-5}
CW	NT	2.27	5.22	6.31×10^{-5}	1.09×10^{-4}
CW	BB	5.14	8.08	7.66×10^{-5}	1.75×10^{-4}

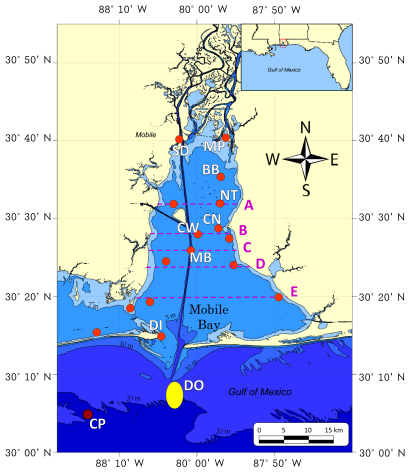

Figure 1. Map of Mobile Bay with color contours marking the 2, 5, 10 and 20m isobath and the location of the offshore mooring (maroon dot), estuary water quality stations (red dots), hydrographic surveys transects (dash lines), and additional offshore hydrographic survey sites (yellow dot).

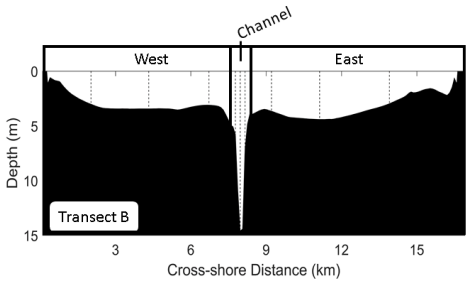

Figure 2. Cross section view of Mobile Bay at transect B where dashed vertical lines show CTD profile locations and grouping of east, west, and channel sections.

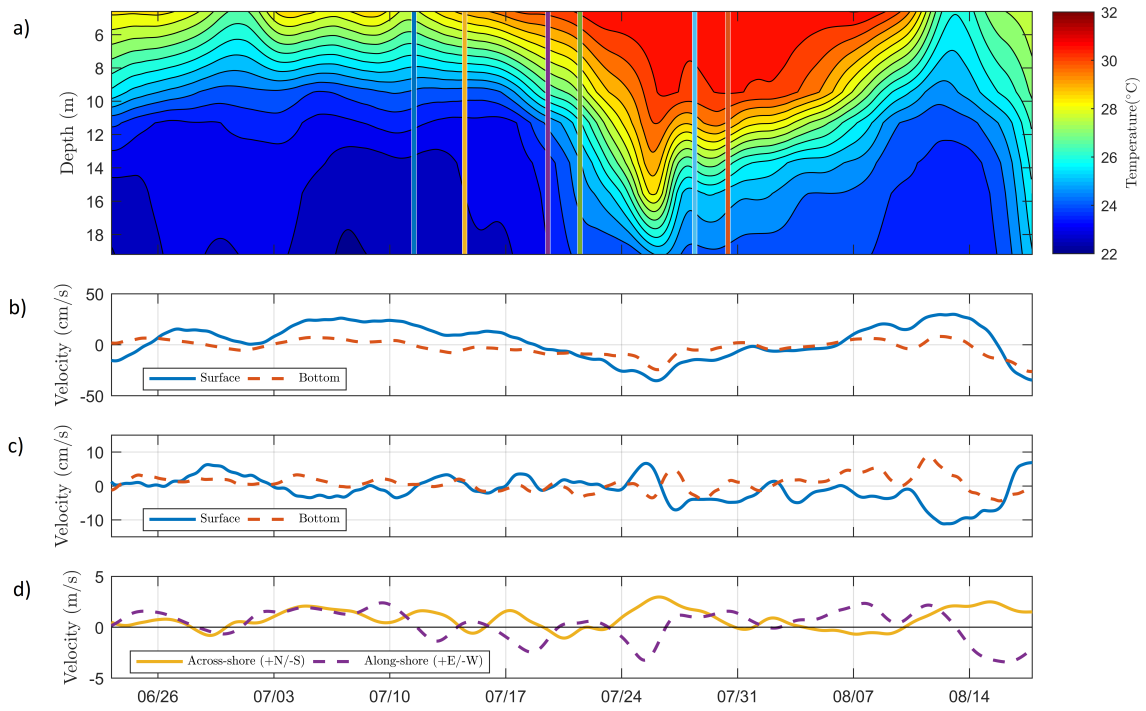

Figure 3. Subtidal timeseries at offshore station CP: (**a**)Temperature, vertical lines denote transect survey dates, (**b**) Along-shelf current velocity (East-West), (**c**) Across-shelf current velocity (North-South), and (**d**) cross and along-shelf wind velocity (in the direction of travel).

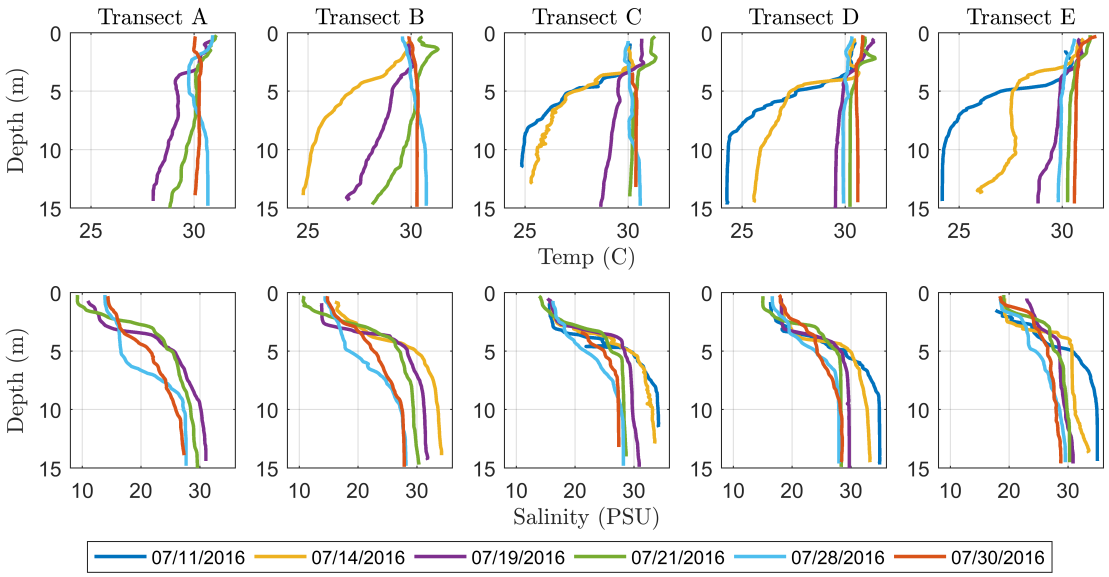

Figure 4. Vertical temperature and salinity profiles in the shipping channel (from lines A-E). Changes show the variability in temperature and salinity starting on July 11th (just after an upwelling event) through July 30th (towards the end of a downwelling event).

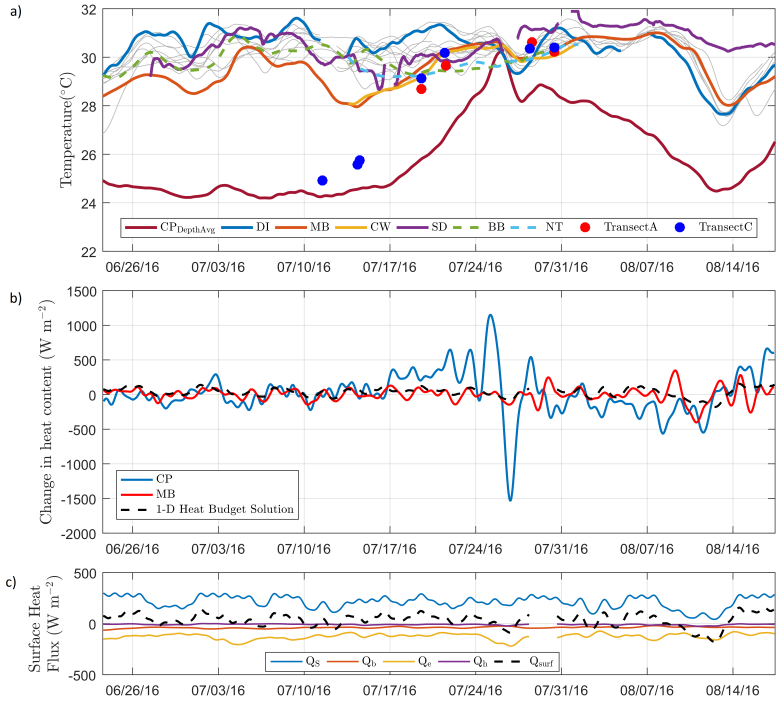

Figure 5. Subtidal timeseries from Mobile Bay: (**a**) Temperature, gray lines denote all the temperature data from unspecified stations to highlight the difference between the two upwelling events, and transect A and C are near bottom temperatures in the shipping channel based on hydrographic survey data, (**b**) change in heat content at stations CP, MB, and a 1-D (no advection model solution) (**c**) surface heat flux components at station MB: shortwave, longwave, latent, and sensible heat flux.

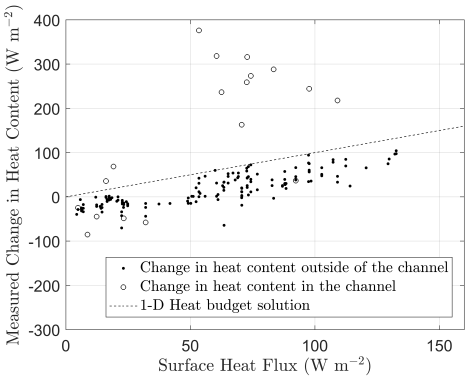

Figure 6. Heat content change calculated from individual CTD profiles throughout Mobile Bay. Black dots are profiles outside the channel and open circles are profiles in the shipping channel. The dashed line assumes a 1-D model solution with no advection.

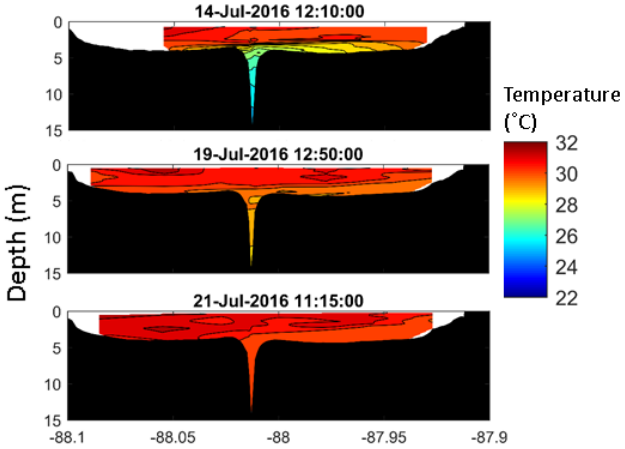

Figure 7. Cross-bay temperature profiles at Transect B highlight the relatively cold-water changes in the channel and in the shallow regions of the bay 30 km from the mouth of the estuary.

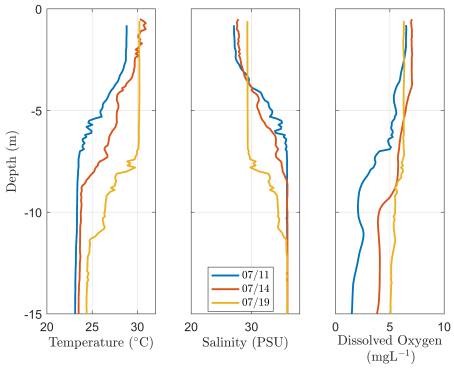

Figure 8. Dissolved oxygen, temperature, and salinity offshore showing the changes during and immediately after the upwelling event.

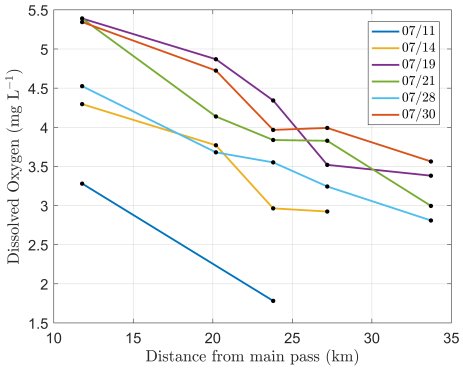

Figure 9. Dissolved oxygen below the pycnocline (5-11 m) in the shipping channel is plotted as a function of distance from the mouth of the estuary. The lowest dissolved oxygen concentration occurs on 7/11 and increases as the upwelling event ends.

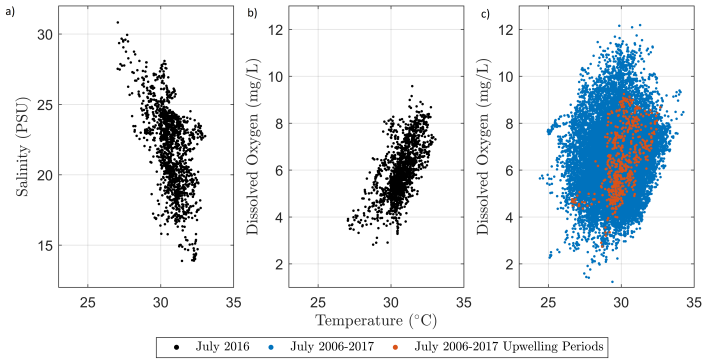

Figure 10. Temperature data from the DI station plotted with (a) salinity for the month of July 2016, (b) dissolved oxygen for the month of July 2016, and (c) dissolved oxygen for the month of July 2006-2017 where blue marks all the available data and red highlight periods of offshore transport and upwelling.